Results in Engineering 28 (2025) 106927

Contents lists available at ScienceDirect

Results in Engineering

journal homepage: www.sciencedirect.com/journal/results-in-engineering

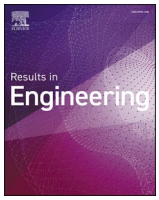

Research paper

DualSPHysics simulations of various wave-structure interactions

Haixin Lu [a], Yu Zheng [a,b], Huabin Shi [c], Matteo Rubinato [d], Songdong Shao [a,b,*]

[a] School of Environment and Civil Engineering, Dongguan University of Technology, Dongguan 523808, China
[b] Guangdong Provincial Key Laboratory of Intelligent Disaster Prevention and Emergency Technologies for Urban Lifeline Engineering, Dongguan University of Technology, Dongguan 523808, China
[c] State Key Laboratory of Internet of Things for Smart City and Department of Ocean Science and Technology, University of Macau, Macao 999078, China
[d] Department of Civil Engineering, College of Engineering and Physical Sciences, Aston University, Birmingham B4 7ET, United Kingdom

ARTICLE INFO

Keywords:
SPH
DualSPHysics
MoorDyn
Wave-structure interaction
Ocean engineering

ABSTRACT

With rapid advancement in ocean engineering, the accurate simulation of interactions between the waves and the structure becomes crucial for optimizing the design process and enhancing the safety and performance of such structures. The present study carries out a series of numerical simulations on wave-structure interactions under three different scenarios using the mesh-free Smoothed Particle Hydrodynamics (SPH) approach, including a fixed, freely floating and moored structure. An open-source code, based on the Dual Smoothed Particle Hydrodynamics Physics (DualSPHysics), is used as the implementation tool. To evaluate the performance of SPH together with the coupled mooring line model, the study compares the computed wave force, free surface elevation, float motion, and mooring forces with the documented data. For the mooring structure case, the RMSE error in computed wave surface elevation is 0.0056 m, 0.001 m in float motion and 0.72° in pitch angle, and 3.1 N in mooring force. The linear correlation coefficients were found to be around 1.0 while the amplitude errors of most physical quantities were in the range of 0.9 - 1.0. Besides, a comprehensive evaluation of key parameters in the model has been carried out to complement the limitations of previous model studies.

1. Introduction

Over the past decades, Computational Fluid Dynamics (CFD) techniques have made significant contributions to simulating the free-surface flows [1], including wave-structure interactions in the ocean engineering field [2,3]. Early frequency-domain analytical methods, typically based on the potential flow theory, often neglect the viscous effect of fluids and nonlinear factors, thus limiting their capacities to solve complex large wave and floating body interactions [4]. To overcome this limitation, researchers have developed numerous models based on the Navier-Stokes (NS) equations or Reynolds-averaged Navier-Stokes (RANS) equations, combining the Finite Difference Methods (FDM) or Finite Volume Methods (FVM) with Volume of Fluid (VOF) for the free surface tracking [5]. These models have effectively simulated the nonlinear interactions between the waves and structures. For example, Hadžić et al [6] predicted the multi-degree-of-freedom motion of a free-floating rectangular body using FVM and grid modeling techniques, while Jung et al [7] simulated the coupled interaction between the waves and freely-rolling rectangular structure. Moreover, Schmitt and Elsaesser [8] employed CFD to investigate the wave-structure interactions of an Oscillating Wave Converter (OWC), optimizing its engineering design and performance. Besides, the naoe-FOAM-SJTU solver developed by Wang et al [9] demonstrated highly-computational accuracy and efficiency in marine hydrodynamic simulations, especially in the ship motion and fluid-structure interactions. However, challenges still remain in the accurate simulation of large-amplitude structural motions and free-surface deformations, particularly under the complex and extreme ocean climate in engineering practice.

Recently the Smoothed Particle Hydrodynamics (SPH) method emerged as a more promising numerical solution [10]. The SPH method, a totally mesh-free numerical technique based on the Lagrangian framework, is naturally suited to handle the large free-surface deformations and complex wave-structure interactions [11]. Unlike traditional Eulerian methods, SPH can avoid the grid distortion issues and exhibit high computational stability when simulating the large-scale flow with free surfaces. Significant progresses have also been made in simulating the wave impact, liquid sloshing and wave-structure coupling. Crespo et al [12] simulated a dam-break phenomena using SPH, establishing its foundation in the large-scale free-surface flow

* Corresponding author.
E-mail address: songdongshao@hotmail.com (S. Shao).

https://doi.org/10.1016/j.rineng.2025.106927
Received 19 June 2025; Received in revised form 30 July 2025; Accepted 24 August 2025
Available online 25 August 2025
2590-1230/© 2025 The Authors. Published by Elsevier B.V. This is an open access article under the CC BY license (http://creativecommons.org/licenses/by/4.0/).

studies. Gao et al [13] and Ren et al [14] used the SPH for wave slamming on a submerged pile, and wave interaction with a porous breakwater, respectively. It should also be mentioned that He et al [15] used the predecessor of DualSPHysics, i.e. SPHysics, for the study of moored multi-float breakwater motions under the regular wave actions, and they validated the results using extensive experimental data.

Since its initial application, SPH method has achieved wide popularity in the fluid mechanics, structural mechanics and biomechanics fields [16]. The development of open-source code, DualSPHysics [17] significantly enhanced the practical application of SPH in ocean engineering. As a GPU-accelerated SPH technology using CUDA, DualSPHysics has become a competitive choice in the wave-structure interaction study due to its outstanding computational performance. Moreover, DualSPHysics also supports the coupling with other numerical tools, such as the wave propagation model and the Discrete Element Method (DEM), thereby broadening its applicability in the coastal and offshore fields. It should be noted that the integration of MoorDyn module [18] with DualSPHysics has further enhanced its capacity to investigate the dynamic responses of floating structure, which can effectively handle the free-surface waves, complex geometric structures, and nonlinear dynamic responses. For example, Dominguez et al [19] were the first to couple DualSPHysics with the dynamic mooring analysis software MoorDyn, effectively simulating the motion of a floating structure under waves. Following this, Liu and Wang [20] optimized the design of a submerged box-type floating breakwater, demonstrating that the dual rectangular breakwaters exhibit the best wave attenuation performance. Han and Dong [21] investigated the performance of a floating breakwater with protruding plates, through a combination of the laboratory experiment and numerical simulation, and they found that the horizontal protruding plate could effectively suppress the oscillations. Some other recent DualSPHysics applications include Yang et al [22], who developed a novel wave-current open boundary module into DualSPHysics to address complex waves on variable sheared currents in practical marine environment. González-Ávalos et al [23] used an integrated model of DualSPHysics and MoorDyn for evaluation of hydrodynamic forces on a copper alloy aquaculture net, such as a fish cage floating over a unidirectional flow. Mostly recently, Ruffini et al [24] coupled SPH with a Discrete Element Method based model, Project CHRONO, to predict the debris dispersion features of different initial configurations during extreme hydrodynamics event. However, while a few explorations have been made into coupling between DualSPHysics and MoorDyn, more comprehensive performance studies on the float motion and mooring line response remain limited.

The present study conducts numerical simulations using the standard DualSPHysics - MoorDyn model, for various wave-structure interaction scenarios, i.e. where the structure is fixed, free floating or moored floating. The research focuses on evaluating the model performance under different hydrodynamic and structure conditions. Through examining the numerical accuracy in wave profiles, structural motions and hydrodynamic forces, we carried out an extensive model validation and accuracy enhancement through sensitivity analyses of particle resolution, optimal kernel range, mooring line stiffness and segment, and flow viscosity etc. In summary, a comprehensive evaluation of key parameters in DualSPHysics-MoorDyn model has been carried out in this work to complement the limitations of previous model studies.

The paper is structured as follows: Section 2 presents governing equations and numerical methods of SPH, along with the summary of DualSPHysics-MoorDyn coupled model. Section 3 devotes to SPH simulations of two wave-structure interaction problems, including fixed and free-floating boxes. Section 4 dedicates to challenging simulations of a moored floating structure in waves, including a sensitivity analysis of several key model parameters. Finally, Section 5 concludes the work and addresses the limitation of study for future research needs.

2. SPH governing equations and numerical methods

The Smoothed Particle Hydrodynamics (SPH) method simulates the dynamic behavior of fluids using particles. These particles carry physical quantities such as position, velocity, density, and pressure, which are computed through the interpolation based on the neighboring particle values. The Lagrangian nature of SPH allows for the simulation of free-surface flows without the need of specialized surface treatment, thereby naturally enabling the multi-domain connectivity of a computational area involving different material media.

DualSPHysics is an open-source solver based on the Weakly Compressible SPH (WCSPH), specifically designed to address practical engineering problems of large scale. It utilizes an equation of state to model the fluid pressures, and imposes a flexible dynamic boundary condition to handle complex geometries of the fluid-driven structure. DualSPHysics is a set of *C++*, CUDA and Java codes with highly computational efficiency, which is executed on the Graphic Processing Unit (GPU) platform. Here a brief summary is reviewed on the fundamental SPH method and DualSPHysics code.

2.1. SPH governing equations

The SPH method is a mesh-free Lagrangian computational technique that solves partial differential equations by discretizing the fluid into numerous particles. The foundation of SPH approach lies in the use of kernel functions to interpolate the interactions between particles. The momentum equation and the mass continuity equation describe the velocity variation and density evolution of the fluid particles, respectively. The Navier-Stokes equations can be expressed in the discrete SPH form as follows:

Momentum equation:

$$\frac{d\mathbf{v}_a}{dt} = -\sum_b m_b \left(\frac{P_b + P_a}{\rho_b \rho_a} + \Pi_{ab} \right) \nabla_a W_{ab} + \mathbf{g} \tag{1}$$

Mass continuity equation:

$$\frac{d\rho_a}{dt} = \sum_b m_b \mathbf{v}_{ab} \cdot \nabla_a W_{ab} + 2\delta_\Phi h c_0 \sum_b (\rho_a - \rho_b) \frac{\mathbf{r}_{ab} \cdot \nabla_a W_{ab}}{{\mathbf{r}_{ab}}^2} \frac{m_b}{\rho_b} \tag{2}$$

where t represents the time, $\mathbf{v}$ the velocity, P the pressure, ρ the density, m the mass, $\mathbf{g}$ the acceleration due to gravity, c the speed of sound, $\mathbf{r}$ the position, and Π_{ab} the viscous term. The kernel function W_{ab} value depends on the normalized distance between reference particles a and neighboring b. In this study, a quintic Wendland kernel function is employed. h is the smoothing length and the kernel function vanishes when the particle separation distance exceeds $2h$. The second term on the right-hand side of Eq. (2) represents the density diffusion term proposed by Molteni and Colagrossi [25]. This term effectively reduces the density fluctuations caused by the rigid density field and the inherent disorder of Lagrangian perspective. According to DualSPHysics common practice, a coefficient $\delta_\Phi = 0.1$ is adopted in this study.

In DualSPHysics, the fluid is considered to be weakly compressible, and thus the fluid pressure is determined using the Tait equation of state, which relates the pressure and density according to the following expression:

$$P = b\left[\left(\frac{\rho}{\rho_a} \right)^\gamma - 1 \right] \tag{3}$$

where $b = {c_0}^2 \rho_0 / \gamma$, with $\gamma = 7$ and $\rho_0 = 1000$ kg/m^3 for the water. The sound speed c_0 at the reference fluid density is controlled to be at least 10 times larger than the maximum fluid velocity, ensuring that the density variation remains below 1 %.

It should be noted that the above governing equations, i.e. Eqs. (1) - (3) are presented in a code-centric view. This form is applicable to both 2D and 3D flow applications with different wave tank layouts and solid

boundary conditions, while the shallow-water equations (SWE) based SPH instead takes a completely different form.

The Dynamic Boundary Conditions (DBC) proposed by Crespo et al [26] are adopted to treat various types of solid walls. By using this DBC, the wavemaker can be treated as a moving boundary, with its motion being predefined by the wave generation theory. Besides, there are two different wave absorption methods used in the SPH model, i.e. active and passive absorptions. The former is realized by adding a correction of velocity and displacement to the wavemaker, while the latter employs a damping zone at the end of wave tank. These two wave absorption approaches can be used either separately or collectively. The velocity adjustment in the damping zone is given by the following equation:

$$\mathbf{v} = \mathbf{v}_0\left(1 - \Delta t\beta_r\left(\frac{x - x_0}{x_1 - x_0}\right)^2\right) \tag{4}$$

where $\mathbf{v}_0$ represents the initial velocity of particle when entering the damping zone, while $\mathbf{v}$ is the on-site velocity along the damping zone. x_0 and x_1 correspond to the start and end positions of damping zone, respectively. Δt denotes the time step in SPH simulation, and β_r is a deceleration coefficient used to control the velocity adjustment.

2.2. Motion of floating structures

In SPH approach, by integrating the forces exerted from surrounding fluid particles and applying them to the structure, the motion of a floating body can be easily determined. Firstly, the unit mass force acting on each boundary particle k can be expressed as:

$$\mathbf{f}_k = \sum_{a \in fluid} \mathbf{f}_{ka} \tag{5}$$

where $\mathbf{f}_{ka}$ represents the force per unit mass exerted by the fluid particle a on the boundary particle k.

For the motion of a free moving body, the updates on the linear and angular velocities of the entire object follow the equations:

$$M\frac{d\mathbf{V}}{dt} = \sum_{k \in boundary} m_k \mathbf{f}_k \tag{6}$$

$$I\frac{d\boldsymbol{\Omega}}{dt} = \sum_{k \in boundary} m_k(\mathbf{r}_k - \mathbf{R}_0) \times \mathbf{f}_k \tag{7}$$

where M represents the mass, I the moment of inertia, $\mathbf{V}$ the linear velocity, $\boldsymbol{\Omega}$ the angular velocity, and $\mathbf{R}_0$ the center of mass, of the whole solid object. By performing the integration on Eqs. (6) and (7), the velocity $\mathbf{u}$ of each boundary particle surrounding the structure can be updated as:

$$\mathbf{u}_k = \mathbf{V} + \boldsymbol{\Omega} \times (\mathbf{r}_k - \mathbf{R}_0) \tag{8}$$

2.3. Coupled SPH-MoorDyn

MoorDyn is an open-source software developed by Hall [18] for mooring line dynamics, and the coupling between DualSPHysics and MoorDyn is achieved through a loose coupling strategy. The process initiates with DualSPHysics, which computes the hydrodynamic loads acting on the float, then subsequently transmits the position and velocity data of the float to MoorDyn. Utilizing this information, MoorDyn models the dynamic behavior of the anchor chain, calculates the resulting reaction forces, and eventually transfers the feedback to DualSPHysics. In turn, DualSPHysics integrates these reactions forces derived from both the anchor chains and the fluid dynamics, and updates the motion of the floating structure. This iterative process guarantees that intricate interactions between the fluids and mooring system are accurately captured, while simultaneously maintains computational efficiency. Fig. 1 visually represents the comprehensive coupling flowchart between DualSPHysics and MoorDyn as implemented in this research.

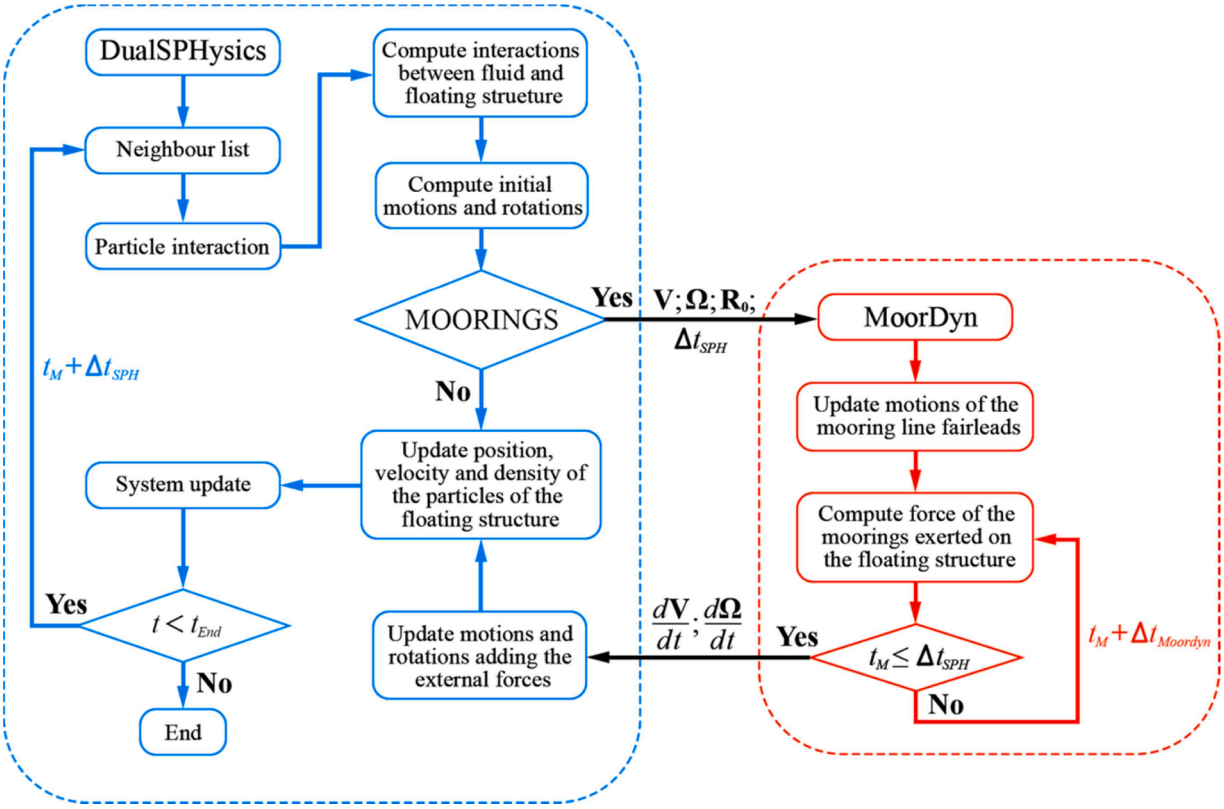

Fig. 1. Coupling process of DualSPHysics with MoorDyn.

2.4. Mooring line and lumped mass models

The motion of the floating structure follows Newton's second law, with the resultant external forces from the surrounding fluid particles. The mooring lines function to prevent excessive drift of the float by constraining its six-degree of motion. The floating structure is anchored to the seabed by a mooring chain, which has two key endpoints: one is fixed to the seabed, and the other is connected to the mooring point on the floating structure.

The dynamic behavior of the mooring line is modeled using the so-called lumped mass approach. This method divides the chain into N equal-length segments and these are connected with $N+1$ nodes. The net weight, buoyancy, internal forces, damping forces, drag forces, and added mass at each node are calculated using the method of Hall and Goupee [27]. Based on these calculations, the acceleration of the nodes is determined by solving the force balance equation, which is then used to update the nodes' velocities and positions, ultimately obtaining the overall dynamic response of the floating structure.

Fig. 2 schematically shows the mooring line and lump-mass models employed in the present DualSPHysics computations.

3. Model applications and results analyses

The purpose of studies in the following sections is twofold: firstly, to evaluate the accuracy of DualSPHysics in wave applications, based on the wave forces acting on the fixed structure and the motion of a free-floating object; secondly, to evaluate the robustness of DualSPHysics-MoorDyn coupled model in simulating the interactions between the waves and a moored floating structure. Three 2D SPH computations are implemented in the present section for a fixed, free-floating and moored floating structure. It should be mentioned that the following adopted wave conditions are mostly laboratory scale and could only represent smaller ocean waves in practical field. However, with the increasing computing power, the model can be easily extended to larger wave problems without any technical constraint.

3.1. Interaction of waves with a fixed surface-piercing structure

Fig. 3 shows the numerical setup for the test case. The model configuration follows the study outlined by Ren et al [28], featuring a fixed rectangular box measured 0.63 m in length and 0.15 m in height, and being partially submerged in water. The box is positioned within the Numerical Wave Tank (NWT), located 2.0 m from the wave generator at the upstream boundary, and 0.3 m from the wave absorbing layer at the downstream boundary. The model incorporates both an active wave absorbing generator and a passive viscous wave absorbing layer, for generating and absorbing the wave energy, respectively.

The wave pressures are recorded at nine measurement points distributed across the surface of the box, with their positions listed in Table 1. The coordinate system is defined with the origin being paced at the bottom of the left wave tank, with positive x-axis pointing to the right, and positive z-axis pointing upwards.

The present SPH simulations use regular waves with a wave period of 1.0 s and wave height of 0.1 m Two different particle spacings are used in the numerical simulations (dp = 0.01 m and dp = 0.005 m). Accordingly, 35,042 and 133,703 particles are generated at these two

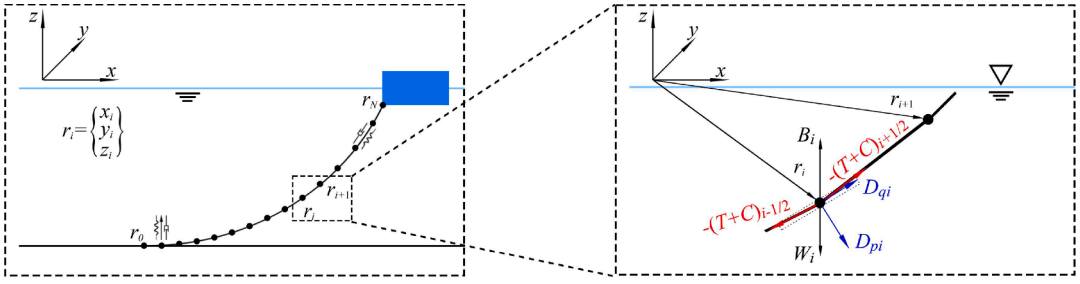

Internal force	$C_{i+1/2}$: Damping force $T_{i+1/2}$: Tension W_i : Weight
External force	D_{qi} : Tangential drag force D_{pi} : Transverse drag force B_i : Buoyancy

Fig. 2. Sketch of the mooring line model and lumped-mass method in MoorDyn.

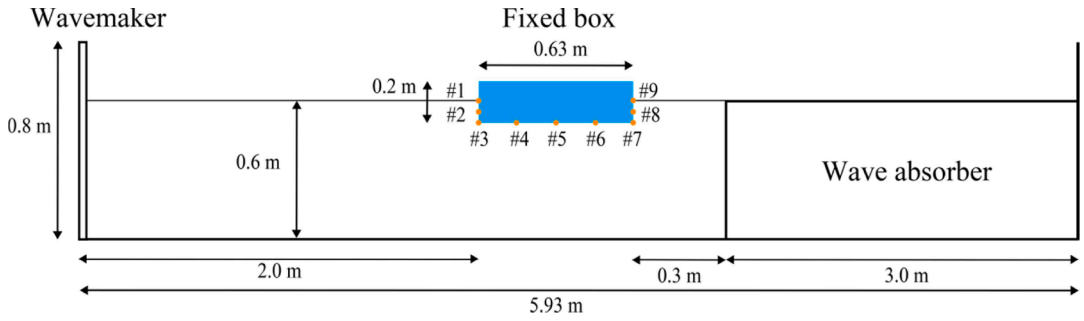

Fig. 3. Numerical setup of wave interactions with a fixed box by Ren et al [28].

Table 1
Coordinates of pressure measuring points on the surface-piercing box.

Coordinates	#1	#2	#3	#4	#5	#6	#7	#8	#9
x (m)	2.000	2.000	2.000	2.158	2.315	2.472	2.630	2.630	2.630
z (m)	0.600	0.562	0.525	0.525	0.525	0.525	0.525	0.562	0.600

resolutions, and the computational time required for a 15-second simulation using an NVIDIA GeForce RTX 3060 GPU is 5 min and 12 min, respectively. Fig. 4 shows the hydrodynamic pressure simulation results at nine measurement points on the surface of the box. The SPH results agree with the analytical solutions provided by Mei and Black [29] in terms of the overall trend. Besides, the SPH computations using two different particle resolutions are very close to each other, demonstrating the convergence of the model.

From the pressure profiles at each measuring point, it can be observed that the points near the primary wave action region experience higher pressure amplitudes, indicating a more significant interaction between the waves and the structure. Furthermore, the pressure exhibits distinct periodic variations in accordance with the wave cycle. In contrast, the measurement points located at the rear side of the box show an obvious reduction in the pressure amplitude, displaying a gentle periodic change. It is noted that at points #4 - #6, numerical results demonstrate oscillations of varying degrees, particularly near the pressure peak regions. The refinement in particle spacing did not effectively smooth out the shock wave effects, indicating that the artificial wave absorbing layer at the tank end may not have fully suppressed the oscillations induced by the shock waves. Furthermore, at points #3 - #6, both particle spacing configurations show an underestimation of the pressure at the wave troughs, which may be attributed to strong nonlinear interactions between the wave and the fixed box, leading to

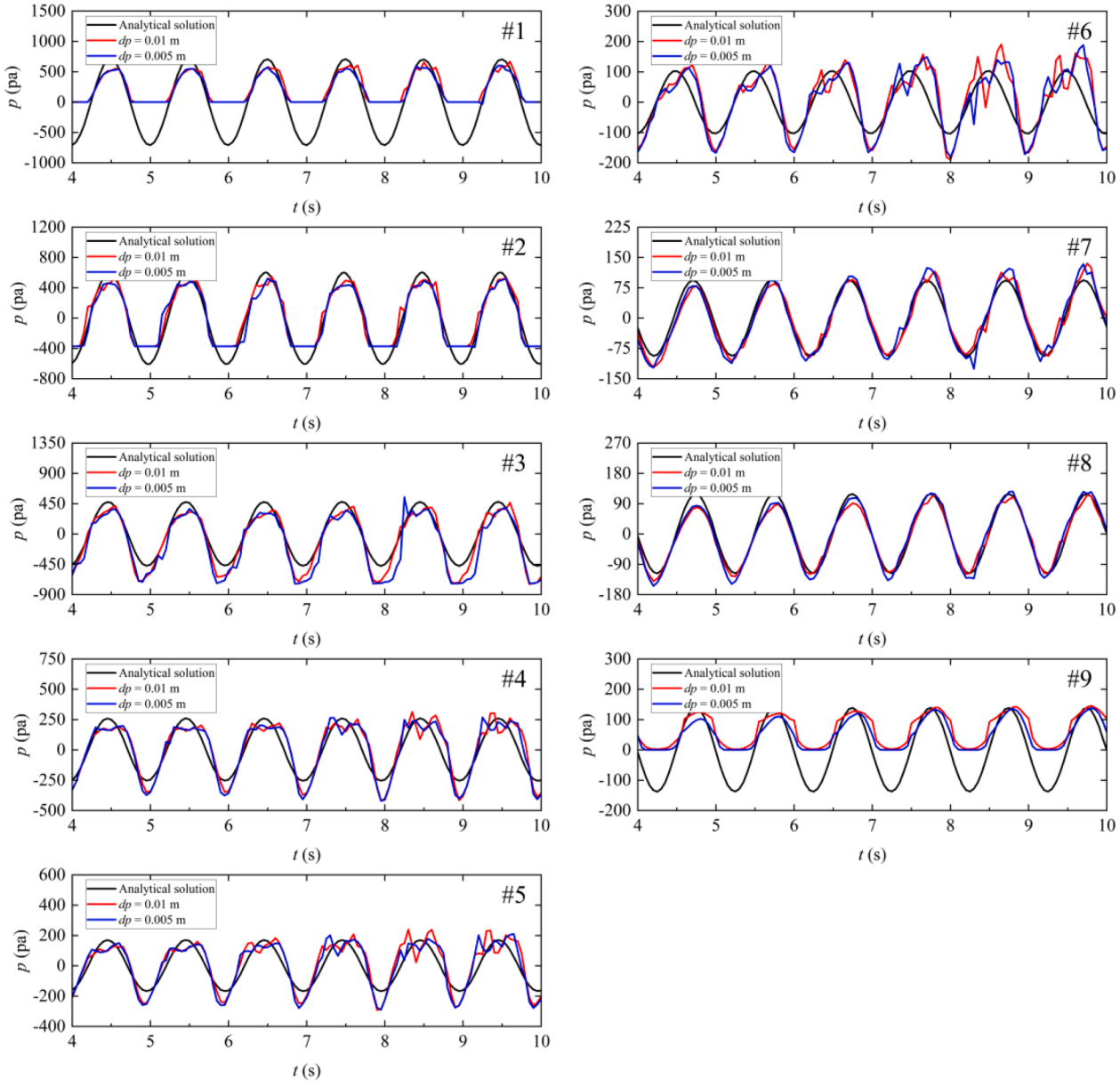

Fig. 4. Comparison of wave pressures on the surface of fixed surface-piercing box: SPH results versus analytical solutions by Mei and Black [29].

inaccurate pressure captures. On the other hand, at the measurement points #1, #2 and #9, where the box is partially exposed outside of the water, the SPH pressure approaches a constant value during the wave troughs. The appearance of negative pressures such as shown in #2 is due to that dynamic pressures are extracted in Fig. 4, which is the subtraction between total pressure and corresponding hydrostatic pressure. Generally, despite some kinds of discrepancy exist, the numerical results are in favorable agreement with the analytical solutions, thus validating the accuracy of DualSPHysics in simulating dynamic wave loads.

3.2. Interaction of waves with a free-floating structure

This section conducts SPH simulation study based on the experimental setup of Ren et al [30]. The general layout of the numerical wave tank (NWT) is illustrated in Fig. 5, with water depth of 0.4 m and a floating box measuring 0.3 m in width and 0.2 m in height. The initial centroid position of the floating body is set at (2.0 m, 0.4 m). In DualSPHysics computation, a piston-type active wave absorber is positioned on the left-side of the tank, while an artificial viscous sponge layer is implemented on the right-side to mitigate wave reflection effects.

The floating body is allowed to undergo three degrees of freedom (DOF) motion, including heaving, surging, and pitching, respectively. Two different particle spacings are used in the numerical simulations (dp = 0.01 m and dp = 0.005 m). Accordingly, 43,640 and 166,256 particles are generated at these two resolutions and the computational time required for a 15-second simulation using an NVIDIA GeForce RTX 3060 GPU is 4 min and 21 min, respectively.

Fig. 6 illustrates the wave elevations at the floating body's location in the absence of the structure, as well as the float's motions of heaving, surging, and pitching after it is placed. A comparison between the numerical and experimental results is conducted to assess the impact of

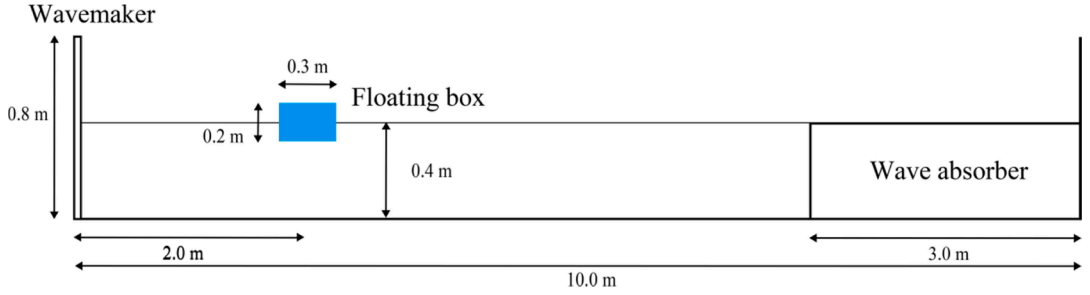

Fig. 5. Numerical setup of wave interactions with a free-floating box by Ren et al [30].

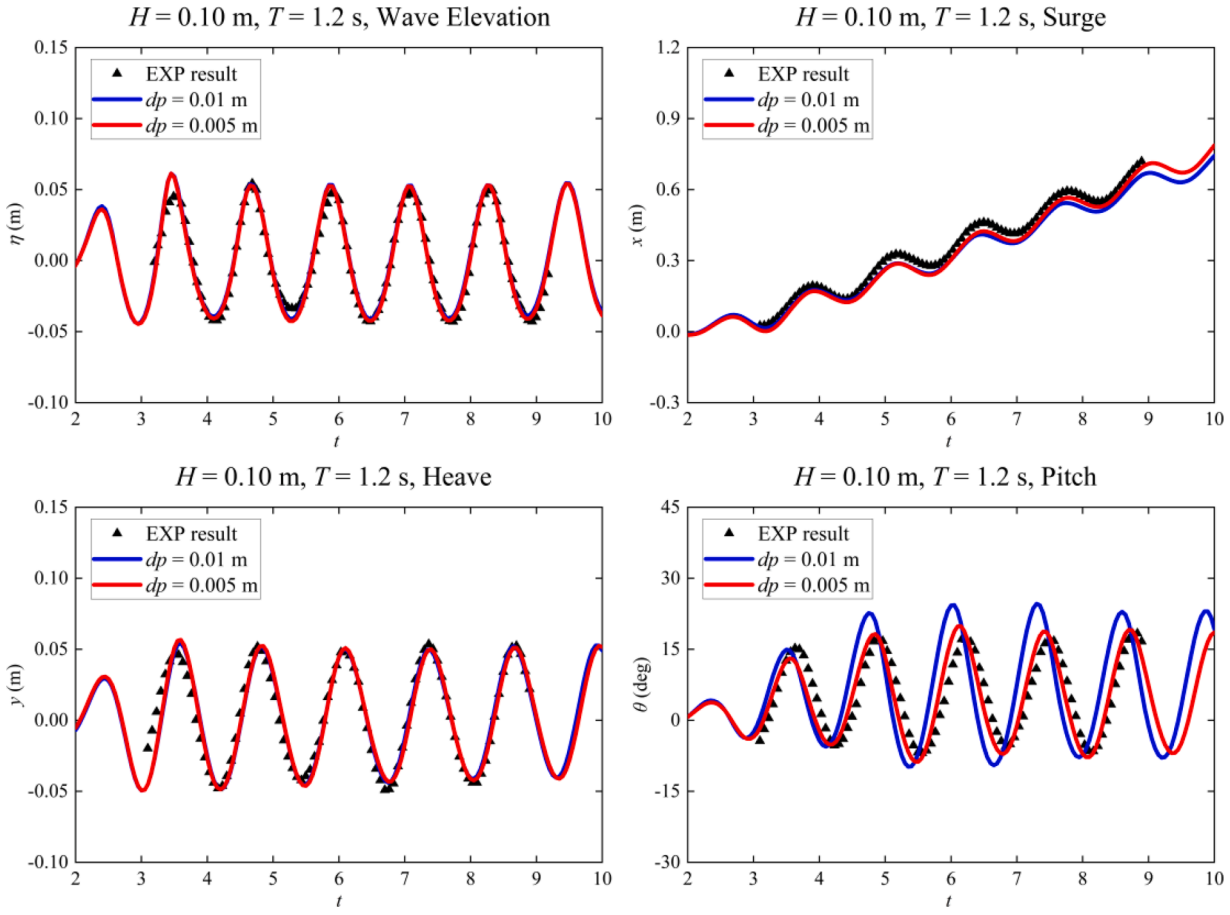

Fig. 6. Comparisons of experimental data and numerical simulations for the motion response of a free-floating box, including the wave elevation, and surging, heaving and pitching of the structure.

resolutions on the dynamic response of the structure. Experimental data were sourced from Ren et al [30]. The top-left panel depicts the wave elevation under $H = 0.10$ m and $T = 1.2$ s conditions, where the numerical results from both particle resolutions exhibit strong agreement with experimental data, as well convergence behaviors.

The top-right panel presents the floating body's surging motion under identical wave conditions. The comparison shows that both low- and high-resolution simulations captured the overall response effectively, but the latter provides a more refined representation of agreement. The bottom-left panel displays the heaving motion, revealing periodic patterns in the vertical displacement. In this instance, there is not much difference observed between the lower and higher resolution results. Moreover, the bottom-right panel compares the time series of pitching angles, where the low-resolution simulations tend to overestimate the peak amplitudes. On the other hand, the high-resolution results more accurately captured the complex dynamics of pitching motion. In this case study, the computational errors mostly arise from inadequate particle resolutions.

Fig. 7 presents the computed horizontal velocity field near the floating box at a resolution of 0.005 m, where the particle colors correspond to the horizontal velocity values. It can be observed that the first and last pictures exhibit nearly the same horizontal velocity field, and an identical orientation of the freely floating box. Surprisingly at time $t_0 + T$, the floating box does not return to its original horizontal position but delays this recovery until $t_0 + 1.12T$. This implies that the motion period of the floating box differs from the incident wave period, and there exists a lagged effect. This phenomenon was also documented in the experiment by Ren et al [30].

To further quantify the agreement between numerical solutions and experimental results, phase error and amplitude error are used for the evaluation. The linear correlation coefficient R is employed to quantify the phase difference between two time-series signals, and defined as follows:

$$R = \frac{1}{\sigma_M \sigma_O} \frac{1}{N} \sum_{n=1}^{N} (M_n - \overline{M})(O_n - \overline{O}) \tag{9}$$

where N represents the number of sample points in the time series, M the

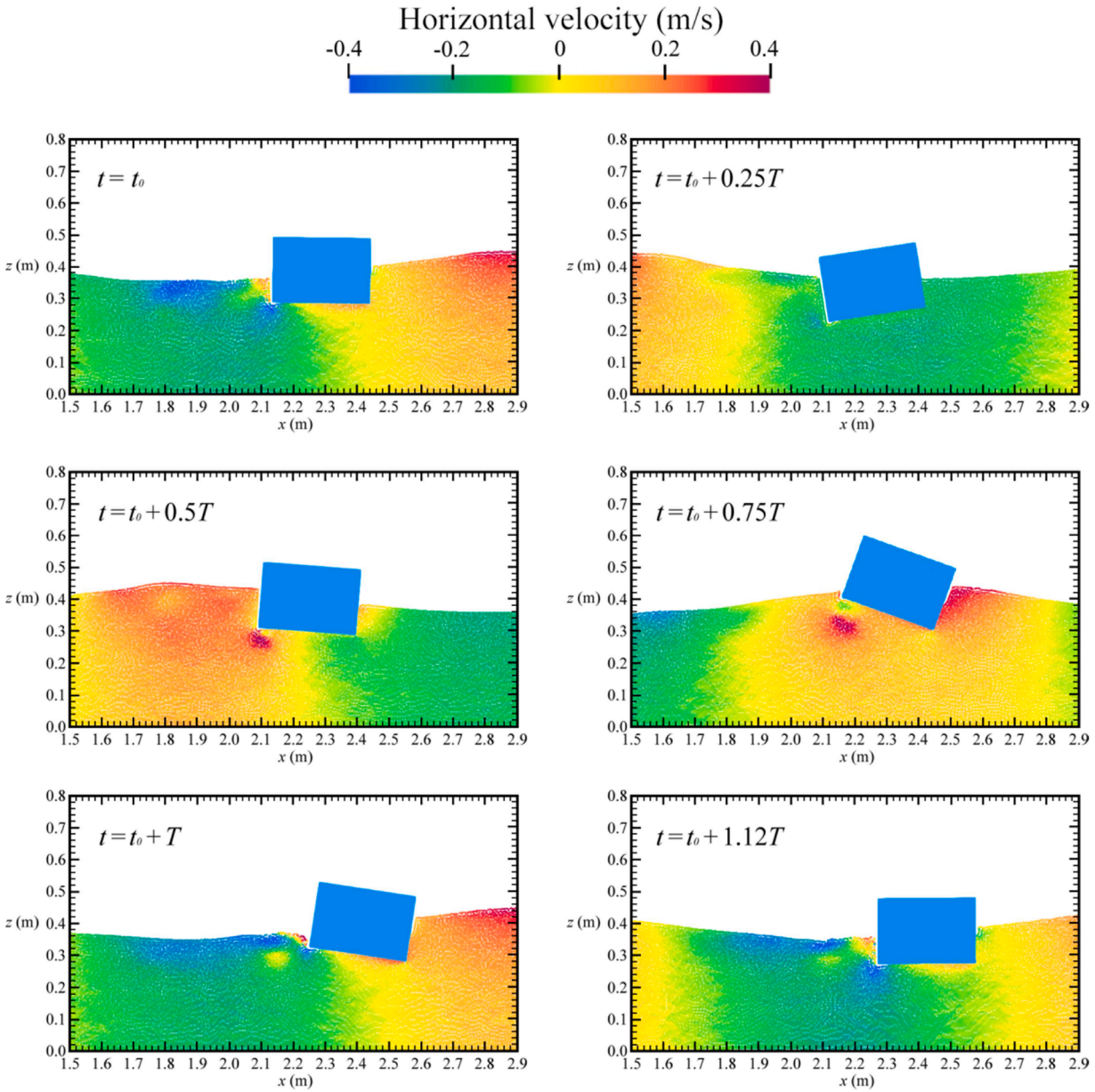

Fig. 7. Particle velocity field of interaction of waves with a free-floating box at different times.

Table 2
Linear correlation coefficient (R) and amplitude error (A) statistics for the freely floating structure.

Parameters	$dp = 0.01$ m		$dp = 0.005$ m	
	R	A	R	A
Elevation (m)	0.98	1.06	0.98	1.06
Heaving (m)	0.96	1.00	0.96	1.01
Surging (m)	0.99	0.91	0.99	0.94
Pitching (°)	0.60	1.29	0.90	1.05

predicted numerical value, and O the experimental observation. σ refers to the standard deviation, and the overline the mean value. When the deviation between model predictions and observed values is negligible, R approaches 1. A negative R value indicates an inverse correlation between the two signals. However, R only captures the phase difference but does not effectively quantify the discrepancies in amplitude. Therefore, an amplitude error A is used as follows:

$$A = \sqrt{\frac{\sum_{n=1}^{N}(M_n)^2}{\sum_{n=1}^{N}(O_n)^2}} \tag{10}$$

Table 2 presents the statistic values of R and A for the numerical results shown in Fig. 6. It is found that, as the particle resolution increases, both the phase and amplitude precisions generally improve, particularly in the surging and pitching cases. Overall, the SPH model demonstrates the ability to enhance numerical accuracy through finer particle resolutions, and well replicates the complex interactions between waves and floating object.

4. Interaction of waves with a moored floating box

The study in this section is based on the wave tank experiment by Peng et al [31] at Nagoya University, Japan. Here SPH model is used to investigate the dynamic responses of a moored rectangular Floating Breakwater (FBW) under regular wave conditions. More comprehensive model validations and sensitivity analyses of parameters are provided to understand the model performance.

4.1. Model setup and computational parameters

The wave tank is 30 m long, 0.7 m wide, and 0.9 m deep, with an initial water depth of 0.6 m. The floating box has a dimension of 0.4 m in length and 0.15 m in height. It has a total mass of 28.6 kg and a moment of inertia of 0.435 kg m^2 about its center of mass. It is anchored to the tank floor by two stainless steel chains each with an inclination angle of 60°, to ensure stability and symmetry of the floating body during the experiment. Four wave probes are positioned at the following locations: 1.95 m, 1.20 m, 1.20 m, and 1.65 m from the center of the breakwater, respectively.

Fig. 8 illustrates the schematic setup of the numerical wave tank, which is equipped with an active wave absorbing piston-type wave maker on the left-hand side to generate regular waves, while an artificial wave absorption zone is located at the opposite end of the tank. The dissipation zone has a length of 2.3 m, designed to absorb outgoing waves and minimize the impact of reflected waves. The adopted wave height is 0.046 m with the wave period 1.0 s.

Table 3
Coordinates of mooring line anchors and fairlead connections. See Fig. 8.

Locations	Points	Coordinates (x, z) (m, m)
Offshore	Anchor A	(2.549, 0.000)
	Fairlead a	(2.750, 0.348)
Onshore	Anchor B	(3.351, 0.000)
	Fairlead b	(3.150, 0.348)

In the numerical setup, the origin of coordinates is set at the bottom of wave paddle on the left side of the tank, with positive x-axis pointing to the right and positive z-axis upwards. The center of mass of breakwater is located at coordinates (2.95 m, 0.423 m), at a distance of 0.102 m between the still water level and top of the breakwater, which is 0.348 m between the bottom of tank and the lower breakwater. The numerical parameters of the float follow Ren et al [28]: total mass 42 kg, moment of inertia at the center of mass 0.64 kg m^2, free length of the anchor chain 0.402 m, and pre-tension of the mooring cable 34.51 N. Table 3 provides the location of cable hooks underneath the breakwater and the anchoring points on tank floor, as shown in Fig. 8.

4.2. Sensitivity analyses of key model parameters

We first conduct a series of convergence tests to evaluate the influence of some key parameters on the numerical results, including particle spacing (dp = 0.02, 0.01, and 0.005 m), kernel function smoothing length ($h = 1.5dp$, $2dp$, and $3dp$), number of mooring segments ($N_m = 5$, 10, and 20), and mooring stiffness ($EA = 8 \times 10^4$, 4×10^5, and 2×10^6 N). Additionally, to further investigate the effect of wave reflection, different artificial viscosity and damping coefficients are also tested to examine the wave propagation characteristics.

Fig. 9(a) – (d) presents the motion series of the float under different test conditions, for the surging, heaving and pitching motions. The results indicate that the particle scale has a significant impact on the simulation accuracy. In the particle spacing test, as dp decreased, the amplitude of surging motion increased, and a more pronounced double-peak motion profile appears in the heaving response. Moreover, the variations in dp also led to noticeable phase differences in all motion responses. When dp was reduced to 0.01 m and 0.005 m, the simulation results became nearly identical, indicating the convergence of results. By balancing both the computational accuracy and efficiency, $dp = 0.01$ m was selected as the reference value for subsequent simulations.

In the kernel smoothing length tests, the changes in h caused slight phase shift in the motion series. The results showed a good convergence when $h = 2dp$. For the mooring segment tests, the motion response was found to be nearly converged at $N_m = 10$, with further increases in segment numbers producing negligible effects. Moreover, in the mooring stiffness tests, when $EA = 8 \times 10^4$ N, insufficient stiffness led to significant mooring line elongation, causing an upward shift in the float's heaving motion. As the stiffness increased, the motion response stabilized at $EA = 4 \times 10^5$ N, indicating that convergence had been

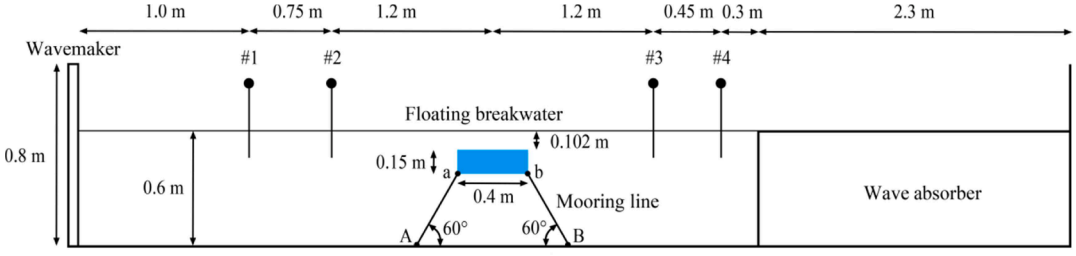

Fig. 8. Numerical setup of wave interactions with a moored-floating box by Peng et al [31].

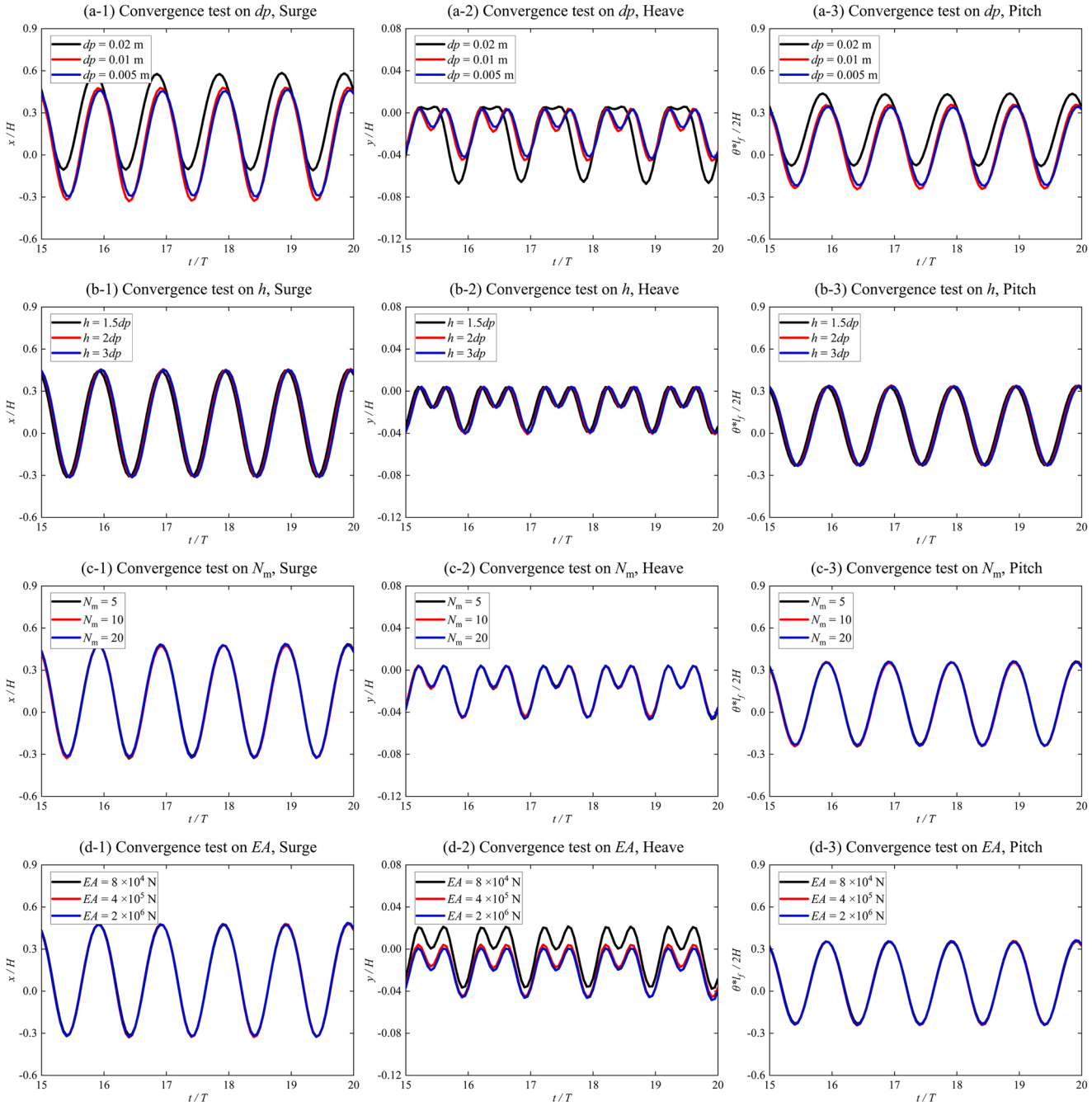

Fig. 9. Motion series of the float in convergence tests (surging, heaving, and pitching): (a) test of particle spacing, *dp*; (b) test of kernel function smoothing length, *h*; (c) test of mooring line segment, N_m; and (d) test of mooring stiffness *EA*.

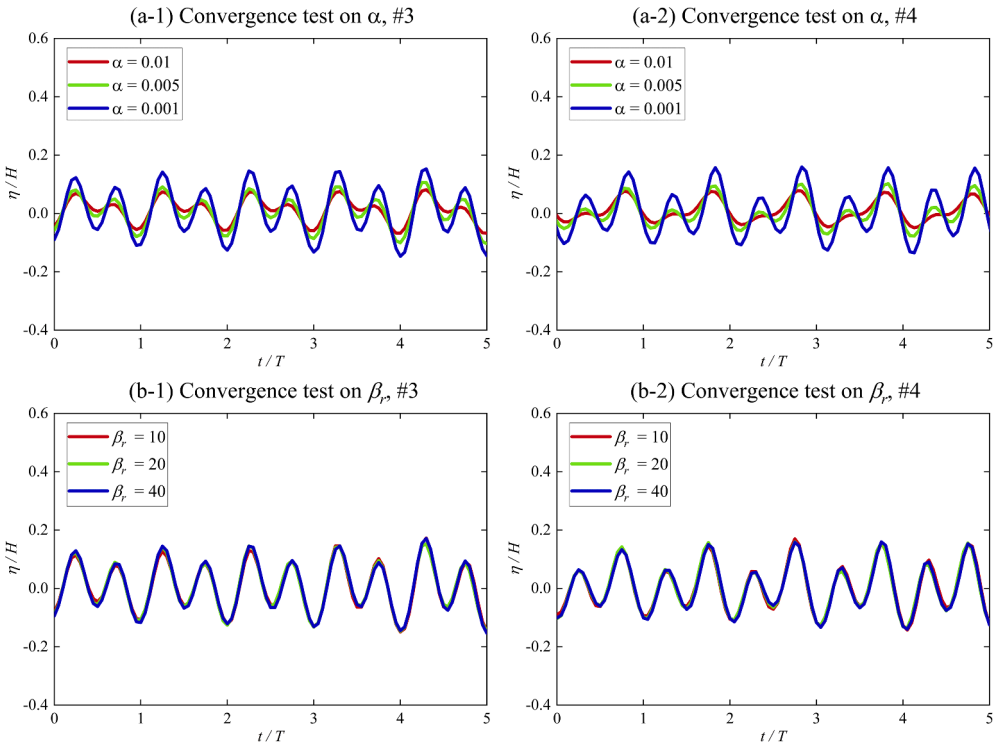

Fig. 10. Free surface elevations at measurement points #3 and #4: (a) tests on artificial viscosity; (b) tests on damping coefficients.

achieved under this parameter.

Fig. 10 shows the variations of free surface elevations at points #3 and #4 with different artificial viscosity and damping coefficients. It can be observed that the complex double-crest wave profile became more distinct as the artificial viscosity coefficient decreased. When $\alpha = 0.001$, the double-crest shape was well captured. In contrast, the wave profile appeared to be relatively insensitive to the changes in the damping coefficient. Therefore, $\beta_r = 20$ was selected as the optimal damping coefficient in this study.

4.3. Model validations and result discussions

Based on the above convergence tests, the final SPH simulation was conducted with the following settings: the particle spacing dp was set to 0.01 m, resulting in a total of 45,185 particles, including 3,494 fixed particles, 450 moving particles, 656 floating particles, and 40,585 fluid particles. The smoothing length of the kernel function was set to $h = 2dp$, with a damping coefficient of $\beta_r = 20$ and an artificial viscosity parameter $\alpha = 0.001$. Table 4 lists the key physical properties of mooring lines used in the simulation. The lines were evenly divided into 10 segments, with each segment having a diameter of 0.003 m, a unit weight of 0.06 kg/m, and an overall mooring stiffness of $EA = 4 \times 10^5$ N.

Table 4
Key parameters of the mooring cable.

Parameters	Values
Segments	10
Mooring line diameter	0.003 m
Mass per unit length	0.06 kg/m
Line stiffness	4.0×10^5 N
Line length	0.402 m

To comprehensively validate this challenging simulation, the SPH wave elevations at positions #1 - #4, the float motions, and mooring line tensions are compared with the experimental data from Peng et al [31] in the following.

Fig. 11 presents the time series of wave surface profiles at locations #1 to #4. The calculated wave elevations are in overall good agreement with the experimental data, with only minor discrepancies observed. On the seaward side, the incident waves induce a clear harmonic motion of the water surface, which is further amplified at certain locations due to the presence of reflected waves. For example, at $t/T = 1.2$, the wave height at measuring point #2 reaches 1.32 times that of the incident wave. On the leeward side, the waves passing through the floating structure undergo significant decomposition, generating higher-order harmonic components. The water surface exhibits pronounced nonlinear characteristics, with steeper and faster changes found in both the wave crests and the wave troughs.

In SPH simulations, the complex double-peaked wave forms observed on the leeward side of the float are also accurately reproduced. However, the calculated wave troughs at points #3 and #4 exhibit a tendency of overestimation. Compared to the results obtained by Ren et al [28] (not provided here), the wave heights simulated by SPH are higher. This discrepancy may be attributed to insufficient damping of the artificial viscosity, which cannot effectively suppress the high-frequency wave components. On the other hand, Ren et al. produced stronger dissipation of the waves that led to an underestimation of wave height due to their viscosity formulation. Overall speaking, the present water surface results show good agreement with the experimental data, demonstrating the accuracy of model for simulating complex moored floating breakwaters.

Fig. 12 presents the computed horizontal velocity field around the breakwater, where the particle colors represent the velocity values. By examining these, a complete cycle of the breakwater's behavior during surging and heaving oscillations is clearly visible. At initial time t_0, the

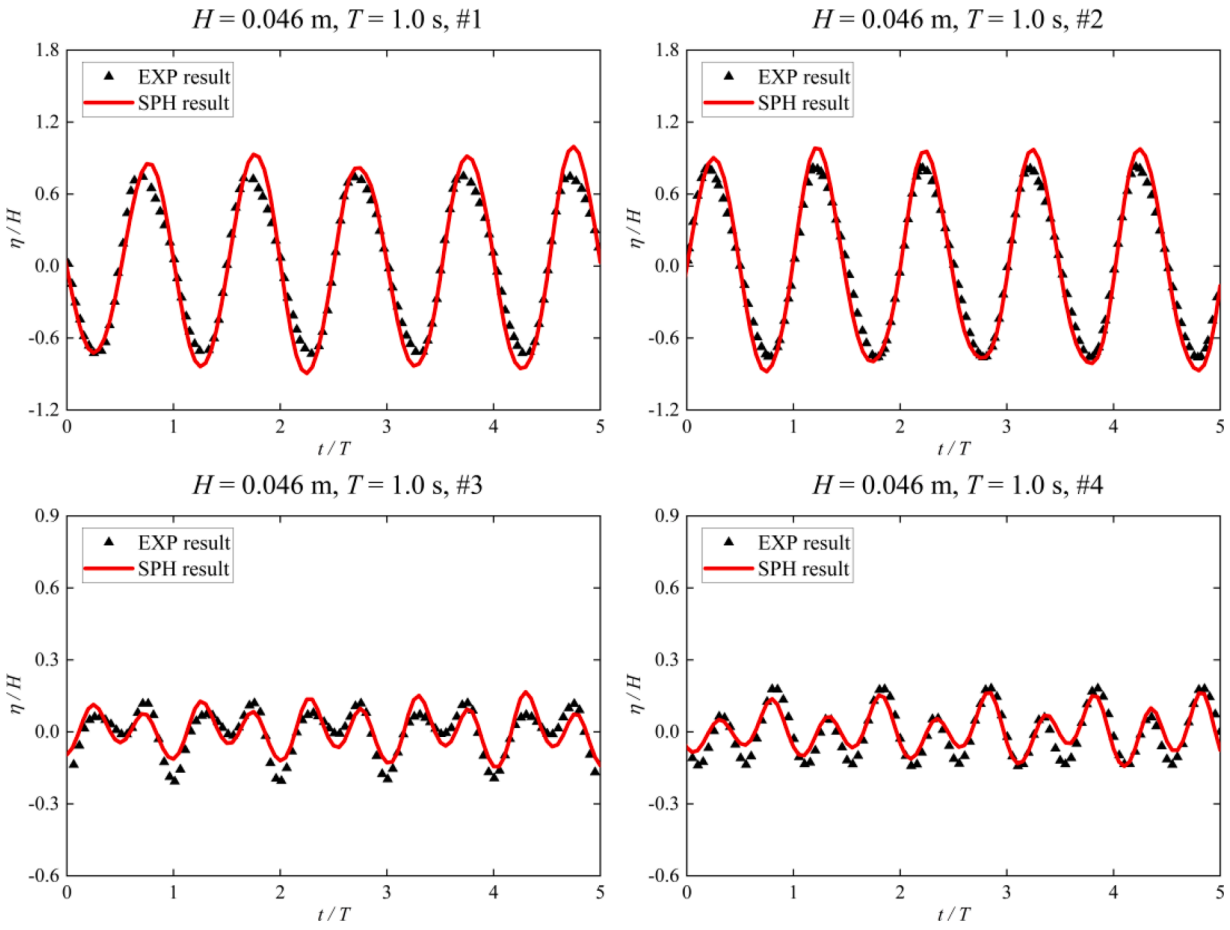

Fig. 11. Comparisons of wave surface elevations from numerical and experimental data at wave gauges #1 – #4.

windward side of breakwater does not show any pronounced wave effect, and the floating body remains almost horizontal. As the wave crest approaches, at $t_0 + 0.2T$, the water surface at the top of breakwater exhibits a depression, and the breakwater begins to rotate clockwise. At $t_0 + 0.4T$, when the wave crest reaches the upper left corner of breakwater, the float undergoes a counterclockwise motion, gradually returning to its original position. By $t_0 + 0.6T$, the wave reaches the top of structure again, and the breakwater rotates counterclockwise from horizontal position, generating a dissipative slope. It is evident that significant nonlinear interactions occur between the incident wave and the breakwater at this moment, resulting in a distortion of transmitted wave height. As time goes on, the changes in particle color at $t_0 + 0.8T$ indicate the occurrence of wave breaking at the top of breakwater, meanwhile, accompanied by secondary wave crests. These secondary waves travel towards the shore at different phase velocities compared with the primary waves. Finally, at $t_0 + T$, the breakwater recovers to the same horizontal state as at time t_0, and the horizontal velocity field is also nearly identical to the original state.

Fig. 13 compares the numerical results of the float's heaving, surging, and pitching motions with the experimental time series. For more clarity, a reference coordinate system, $G - xy$, is defined, where the origin is located at the center of mass of the floating body, and the positive x-axis points to the right and y-axis upward, with counterclockwise rotation being considered as positive. It is shown from Fig. 13 that under the effect of wave crest, the breakwater first moves downwards and to the right, then returns to its equilibrium position. In contrast, under the effect of wave trough, the breakwater moves downwards and to the left before returning to the equilibrium state instead. This phenomenon is also effectively supported by the numerical results as shown in Fig. 12, further confirming that within a wave period, heaving motions exhibit the characteristics of double troughs and crests. From Fig. 13, it is evident that the numerical results from SPH method provide good agreement with the experimental data across all three motion components.

Fig. 14 presents the time series of offshore and onshore mooring forces. It can be observed that the variations in mooring force exhibit a high degree of similarity to the motion patterns of the float heaving component. The results for offshore mooring forces demonstrate an excellent agreement with the experimental data. However, the onshore mooring forces show an overestimation of the force at the second trough, which is due to the relatively poor reproduction of the double-peak characteristics in the heaving motion. Specifically, during the clockwise sinking of the float, the onshore tension force is over-amplified, while during the counterclockwise rising of the float back to its equilibrium position, the tension variation is relatively smoother (see Fig. 12 as well). As a result, the experimental double-peak phenomenon is not fully captured by numerical model. Nevertheless, the coupling effect of SPH and mooring line models has proven to be feasible and shows great potentials in predicting both wave dynamics and structural responses during the wave-float interactions.

Finally, to further quantify the differences between numerical

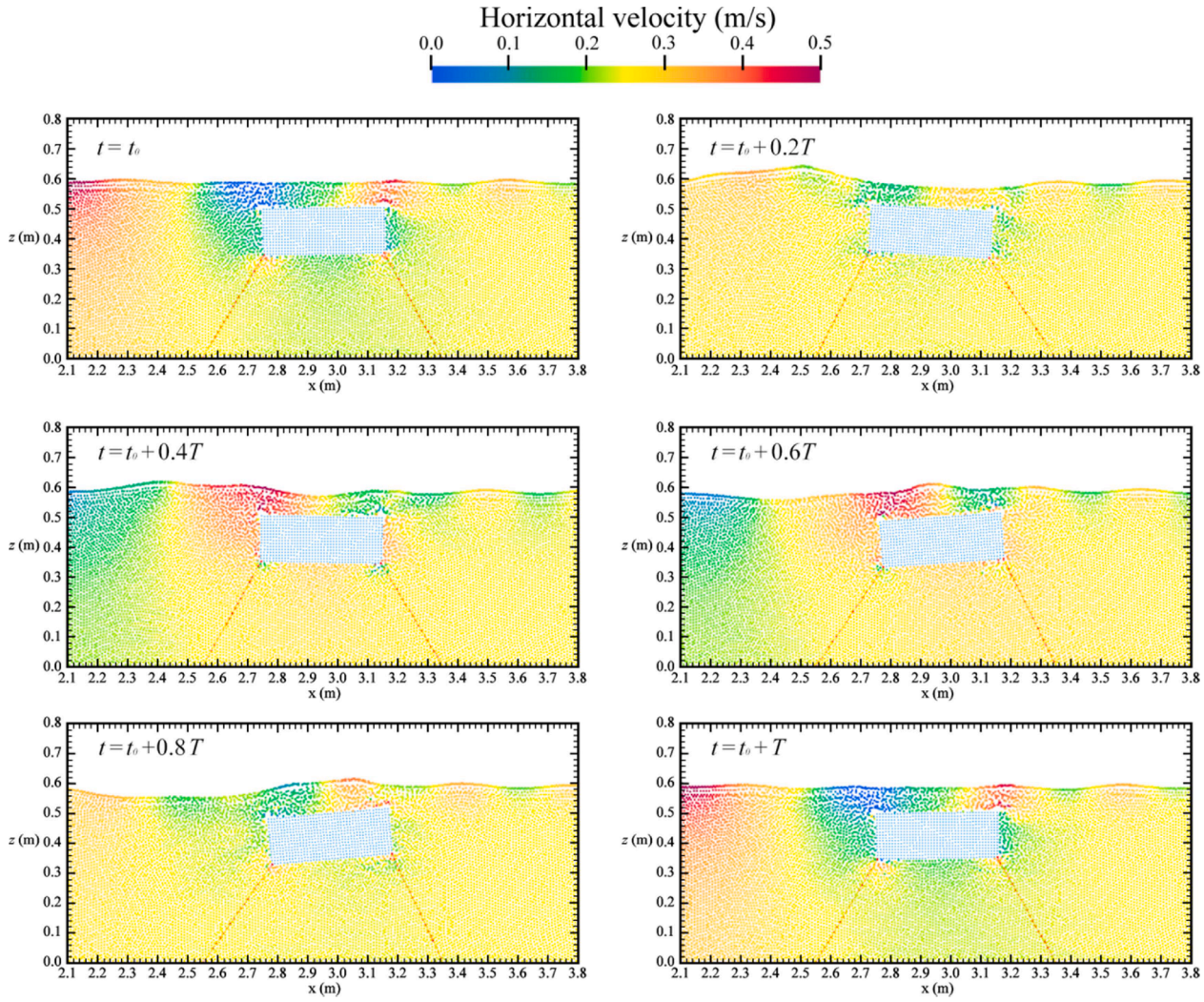

Fig. 12. Particle velocity field of interaction of waves with a moored-floating box at different times.

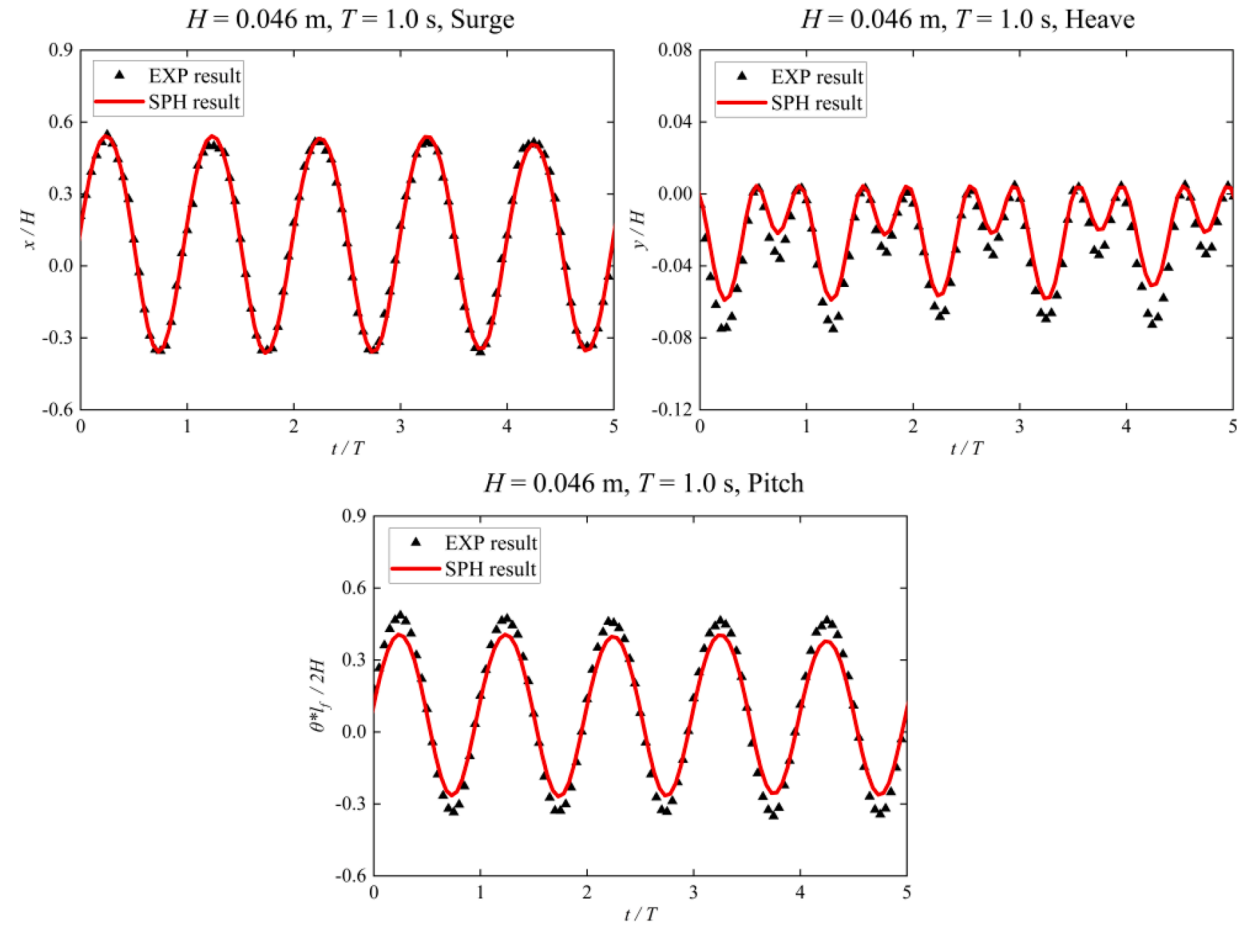

Fig. 13. Comparisons of numerical and experimental results for the motions of moored floating structure in surging, heaving and pitching.

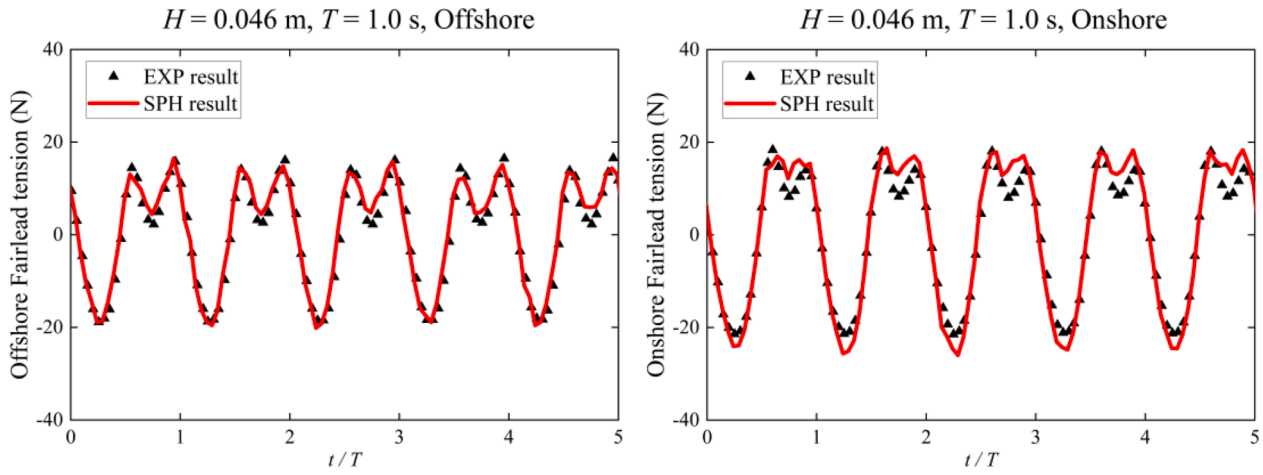

Fig. 14. Comparative analysis of numerical and experimental results for mooring forces.

simulations and experimental data, the linear correlation coefficient R and amplitude error A, as defined in the previous Section 3, are used here to evaluate the time histories of water surface elevation, floating body motion, and mooring forces, as shown in Table 5. It is shown that the experimental results [31] and numerical SPH simulations exhibit satisfactory consistency in most cases. However, certain levels of discrepancies are found in the wave profile at measuring point #4, the heaving motion and the onshore mooring force. These could be attributed to the errors generated from the wave nonlinearity deformation during the wave-structure interactions.

Table 5
Linear correlation coefficient (R) and amplitude error (A) statistics for the moored floating structure.

Parameters		R	A
Surface elevations	# 1	0.99	1.16
	# 2	0.99	1.14
	# 3	0.85	0.87
	# 4	0.92	0.77
Motions of floating structure	Surging	1.00	1.00
	Heaving	0.99	0.76
	Pitching	1.00	0.83
Mooring forces	Offshore	0.98	1.01
	Onshore	0.99	1.16

5. Conclusions

The study examined the performance of DualSPHysics model through three benchmark cases, with different structural constraints. The proposed 2D model is shown to be accurate in predicting the wave surface profiles and floating body motions, effectively capturing the dynamic responses of structure in complex marine environment. The study compares the computed free surface elevation, float motion, and mooring forces with the data. For the moored structure test, the RMSE errors in computed wave surface elevation are 0.0056 m, 0.001 m in float motion and 0.72° in pitch angle, and 3.1 N in mooring force. The linear correlation coefficients were found to be around 1 while the amplitude errors of most physical quantities were in the range of 0.9 - 1.0.

Quite a few numerical computations were also carried out to address the selection of model parameters and the model sensitivity, aiming to apply the model in practical applications where some parameters are difficult to calibrate beforehand. Again, for the moored structure test, a medium particle resolution of 0.01 m with kernel size of $2dp$, mooring line stiffness of 4×10^5 N, and artificial viscosity coefficient of 0.001 were found to provide the best performance in the proposed test settings.

However, some predication errors still remain under specific conditions, such as when the wave nonlinearity is high. Also, the discrepancies in pressure peaks and mooring force amplitudes are noted, particularly under complex wave conditions. These errors could be attributed to the uncertainties in artificial viscosity formulation, mooring line properties, as well as 2D simplifications of real 3D application. Besides, the lack of turbulent modelling also contributed to the numerical errors considering the relatively rough particle resolution.

Considering the rapid development of mesh-free SPH technology during the past two and half decades, it seems the algorithm innovations have reached a stagnation point. Engineering applications should be main direction of SPH subject field. However, practical applications of SPH in large scale always necessitate advanced computing technology, which should constitute one direction of future SPH research.

Nomenclature

The following symbols are used in this paper:
A = amplitude error;
c = speed of sound;
c_0 = speed of sound at reference density;
dp = particle spacing;
EA = mooring stiffness;
$\mathbf{f}_{ka}$ = force exerted by fluid particle a on boundary particle k;
$\mathbf{g}$ = gravitational acceleration;
h = smoothing length;
H = wave height;
I = moment of inertia of solid structure;
m = particle mass;
M = mass of solid structure;
N = number of sample points;
N_m = number of mooring segments;
P = particle pressure;
$\mathbf{r}$ = particle position;
R = linear correlation coefficient;
$\mathbf{R}_0$ = centre of mass of solid structure;
t = time;
t_0 = reference time;
T = wave period;
$\mathbf{u}$ = velocity of boundary particle surrounding solid structure;
$\mathbf{v}$ = particle velocity;
$\mathbf{v}_0$ = initial velocity entering damping zone;
$\mathbf{V}$ = linear velocity of solid structure;
W_{ab} = kernel value between particle a and b;
x_0 = start position of damping zone;
x_1 = end position of damping zone;
α = coefficient in artificial viscosity;
β_r = damping coefficient in wave absorption;
γ = coefficient in equation of state;
δ_Φ = coefficient in density diffusion term;
Δt = time step in SPH simulation;
Π_{ab}= artificial viscosity term;
ρ = particle density;
ρ_0 = reference density of water;
σ = standard deviation;
$\boldsymbol{\Omega}$ = angular velocity of solid structure.

CRediT authorship contribution statement

Haixin Lu: Writing – original draft, Visualization, Validation, Software, Methodology, Data curation. **Yu Zheng:** Writing – review & editing, Supervision, Project administration, Investigation, Funding acquisition. **Huabin Shi:** Writing – review & editing, Project administration, Investigation, Funding acquisition. **Matteo Rubinato:** Writing – review & editing, Resources, Investigation, Conceptualization. **Songdong Shao:** Writing – review & editing, Writing – original draft, Supervision, Methodology, Investigation.

Declaration of competing interest

The authors declare that they have no known competing financial interests or personal relationships that could have appeared to influence the work reported in this paper.

Acknowledgement

This research was funded by National Key Research and Development Program of China (No. 2024FE0201900), The Science and Technology Development Fund (FDCT), Macao S.A.R. (No. 0101/2024/AMJ), and Guangdong Provincial Key Laboratory of Intelligent Disaster Prevention and Emergency Technologies for Urban Lifeline Engineering (2022) (No. 2022B1212010016).

Data availability

Data will be made available on request.

References

[1] K.C. Swami, S.K. Dash, S. Koley, Water waves scattering by floating rigid dock and breakwaters using improved singular boundary method under regular and irregular waves, Results. Eng. 25 (2025) 104420.
[2] A. Alkhalidi, H. Kaylani, N. Alawawdeh, Technology assessment of offshore wind turbines: floating platforms - validated by case study, Results. Eng. 17 (2023) 100831.
[3] A. Asgari, S.F. Ahmadtabar Sorkhi, Wind turbine performance under multi-hazard loads: wave, wind, and earthquake effects on liquefiable soil, Results. Eng. 26 (2025) 104647.

[4] M.S. Longuet-Higgins, E.D. Cokelet, The deformation of steep surface waves on water: I. A numerical method of computation, Math. Phys. Eng. Sci. 350 (1660) (1976) 1–26.
[5] C.W. Hirt, B.D. Nichols, Volume of fluid (VOF) method for the dynamics of free boundaries, J. Comput. Phys. 39 (1) (1981) 201–225.
[6] I. Hadžić, J. Hennig, M. Perić, Y. Xing-Kaeding, Computation of flow-induced motion of floating bodies, Appl Math Model 29 (12) (2005) 1196–1210.
[7] J.H. Jung, H.S. Yoon, H.H. Chun, I. Lee, H. Park, Numerical simulation of wave interaction with a free rolling body, Int. J. Nav. Archit. Ocean Eng. 5 (3) (2013) 333–347.
[8] P. Schmitt, B. Elsaesser, On the use of OpenFOAM to model oscillating wave surge converters, Ocean Eng. 108 (2015) 98–104.
[9] J.H. Wang, W.W. Zhao, D.C. Wan, Development of naoe-FOAM-SJTU solver based on OpenFOAM for marine hydrodynamics, J. Hydrodyn. 31 (1) (2019) 1–20.
[10] J.J. Monaghan, Smoothed particle hydrodynamics, Annu Rev. Astron. Astrophys. 30 (1992) 543–574.
[11] M.B. Liu, G.R. Liu, Smoothed particle hydrodynamics (SPH): an overview and recent developments, Arch. Comput. Methods Eng. 17 (1) (2010) 25–76.
[12] A.J. Crespo, M. Gómez-Gesteira, R.A. Dalrymple, Modeling dam break behavior over a wet bed by a SPH technique, J. Waterw. Port. Coast. Ocean. Eng. 134 (6) (2008) 313–320.
[13] R. Gao, B. Ren, G. Wang, Y. Wang, Numerical modelling of regular wave slamming on subfaces of open-piled structures with the corrected SPH method, Appl. Ocean Res. 34 (2012) 173–186.
[14] B. Ren, H. Wen, P. Dong, Y. Wang, Numerical simulation of wave interaction with porous structures using an improved smoothed particle hydrodynamic method, Coast. Eng. 88 (2014) 88–100.
[15] M. He, D. Liang, B. Ren, J. Li, S. Shao, Wave interactions with multi-float structures: SPH model, experimental validation and parametric study, Coast. Eng. 184 (2023) 104333.
[16] C. Zhang, Y. Zhu, Y. Yu, D. Wu, M. Rezavand, S. Shao, X. Hu, An artificial damping method for total Lagrangian SPH method with application in biomechanics, Eng. Anal. Bound. Elem. 143 (2022) 1–13.
[17] A.J.C. Crespo, J.M. Domínguez, B.D. Rogers, M. Gómez-Gesteira, S. Longshaw, R. Canelas, R. Vacondio, A. Barreiro, O. García-Feal, DualSPHysics: open-source parallel CFD solver on smoothed particle hydrodynamics (SPH), Comput. Phys. Commun. 187 (2015) 204–216.
[18] M. Hall, MoorDyn User's Guide, 15, Department of Mechanical Engineering, University of Maine, Orono, ME, USA, 2015.
[19] J.M. Domínguez, A.J.C. Crespo, M. Hall, C. Altomare, M. Wu, V. Stratigaki, P. Troch, L. Cappietti, M. Gómez-Gesteira, SPH simulation of floating structures with moorings, Coast. Eng. 153 (2019) 103560.
[20] Z. Liu, Y. Wang, Numerical investigations and optimizations of typical submerged box-type floating breakwaters using SPH, Ocean Eng. 209 (2020) 107475.
[21] X. Han, S. Dong, Interaction between regular waves and floating breakwater with protruding plates: laboratory experiments and SPH simulations, Ocean Eng. 287 (2023) 115906.
[22] Y. Yang, S. Draycott, P.K. Stansby, B.D. Rogers, A numerical flume for waves on variable sheared currents using smoothed particle hydrodynamics (SPH) with open boundaries, Appl. Ocean Res. 135 (2023) 103527.
[23] R. González-Ávalos, I. Martínez-Estévez, S. Capasso, J.M. Domínguez, X. Gironella, C. Altomare, Numerical modelling of copper alloy aquaculture net in currents with the Smoothed Particle Hydrodynamics method, Appl. Ocean Res. 151 (2024) 104151.
[24] G. Ruffini, R. Briganti, J. Stolle, P. De Girolamo, Numerical analysis and prediction of the effect of debris initial configurations on their dispersion during extreme-hydrodynamic events, Coast. Eng. 198 (2025) 104702.
[25] D. Molteni, A. Colagrossi, A simple procedure to improve the pressure evaluation in hydrodynamic context using the SPH, Comput. Phys. Commun. 180 (6) (2009) 861–872.
[26] A.J.C. Crespo, M. Gómez-Gesteira, R.A. Dalrymple, Boundary conditions generated by dynamic particles in SPH methods, Comput. Mater. Contin. 5 (3) (2007) 173–184.
[27] M. Hall, A. Goupee, Validation of a lumped-mass mooring line model with DeepCwind semisubmersible model test data, in: Ocean Eng., 104, 2015, pp. 590–603.
[28] B. Ren, M. He, Y. Li, P. Dong, Application of smoothed particle hydrodynamics for modeling the wave-moored floating breakwater interaction, Appl. Ocean Res. 67 (2017) 277–290.
[29] C.C. Mei, J.L. Black, Scattering of surface waves by rectangular obstacles in waters of finite depth, J. Fluid. Mech. 38 (3) (1969) 499–511.
[30] B. Ren, M. He, P. Dong, H. Wen, Nonlinear simulations of wave-induced motions of a freely floating body using WCSPH method, Appl. Ocean Res. 50 (2015) 1–12.
[31] W. Peng, K.H. Lee, S.H. Shin, N. Mizutani, Numerical simulation of interactions between water waves and inclined-moored submerged floating breakwaters, Coast. Eng. 82 (2013) 76–87.